Eur Biophys J (2005) 34: 113–126
DOI 10.1007/s00249-004-0435-y

ARTICLE

Volker Kiessling · Stefano Vassanelli

Potassium channel gating in adhesion: from an oocyte–silicon to a neuron–astrocyte adhesion contact

Received: 23 October 2003 / Revised: 8 June 2004 / Accepted: 5 August 2004 / Published online: 3 November 2004

Abstract In a neuron–astrocyte adhesion contact the ionic current due to the opening of voltage-dependent potassium channels has to flow along a narrow intercellular cleft, generating there an extracellular voltage. This voltage might be large enough to affect significantly the dependence of channel gating from the intracellular voltage. In order to test this hypothesis, we considered a *Xenopus* oocyte expressing voltage-dependent potassium channels adhering to a layer of silicon oxide as a simplified model of cell–cell adhesion; here the cell membrane and silicon oxide are separated by a narrow cleft and form a junction of circular shape. We measured directly the extracellular voltage along the diameter of the cleft and investigated its effect on channel gating using a linear array of field effect transistors integrated in the silicon substrate. On this experimental basis we demonstrated that the voltage dependence of potassium channels is strongly affected by adhesion, as can be predicted using a model of a two-dimensional cable and electrodiffusion theory. Computations based on the model showed that along a neuron–astrocyte adhesion contact the opening of voltage-dependent Kv2.1 potassium channels is significantly reduced with respect to identical channels facing an open extracellular space.

Keywords Adhesion · Extracellular space · Potassium channel · Self-gating · Transistor

Introduction

Voltage-dependent ionic channels play a fundamental role in neuronal signaling. They are responsible for the generation and propagation of the action potential, are involved in synaptic transmission and in the modulation of intracellular molecular signaling.

The gating of voltage-dependent channels is controlled by the voltage difference existing between the two faces, internal and external, of the plasma membrane. It is well known that ionic currents flowing through voltage-gated channels contribute to set the intracellular voltage. On the basis of electrical models, it has been suggested that these currents can also significantly modify the extracellular voltage where cells are in close contact and the extracellular space is reduced to a narrow cleft (Fromherz 1997). In reality, drift and diffusion of ions within the narrow extracellular space might cause changes of extracellular voltage accompanied by modifications of extracellular ionic concentrations (Straub 2001; Fromherz et al., unpublished work). For example, this was suggested to occur because of the opening of potassium channels during action potential propagation in myelinated axons (Frankenhaeuser and Hodgkin 1956; Smith 1983; Inoue et al. 1997; Clay 1998; Zhou and Chiu 2001). As a general consequence, at sites of cell–cell adhesion the dependence of channel gating from the intracellular voltage may differ from regions where the cell faces an open extracellular space. A related effect was postulated, on the basis of a theoretical model, for the current flowing through voltage-independent receptor channels in a single synapse (Savtchenko et al. 2000).

The extracellular voltage developing in a cell–cell adhesion contact with voltage-gated channels has never been experimentally determined. This is mainly because of the technical difficulty of measuring the extracellular voltage in the adhesion cleft between two adhering cells.

A cell adhering to a layer of silicon oxide well reproduces the geometry of a cell–cell adhesion contact with a distance between the cellular membrane and the substrate of a few tens of nanometers (Braun and Fromherz 1998). Also the electrical features are similar: considering that both a silicon oxide layer and a cellular membrane are insulators, a cell–cell as well as a cell–silicon oxide adhesion contact could be electrically

V. Kiessling · S. Vassanelli (✉)
Department of Membrane and Neurophysics,
Max-Planck Institute for Biochemistry,
Martinsried, Germany

Present address: S. Vassanelli
Department of Human Anatomy and Physiology,
Section of Physiology, University of Padua, Padua, Italy

described as a two-dimensional cable (Weis and Fromherz 1997; Kiessling and Fromherz, unpublished work).

Using metal-free field-effect transistors integrated in the silicon substrate as voltage sensors, it has been possible to measure directly the voltage in the adhesion cleft between cell and substrate and the local voltage-dependent membrane conductances (Fromherz 1999; Vassanelli and Fromherz 1999; Straub et al. 2001). In these experiments the intracellular potential was clamped with a patch-clamp electrode in whole-cell configuration and the extracellular voltage beneath the cell was measured by transistors. Owing to the small size of the cells, the extracellular voltage in the cleft was probed only by one or two transistors. Therefore the spatial profile of the voltage along the electric cable could not be measured, but rather only an averaged voltage. An average of the steady-state ionic conductance in the adhering membrane was derived from these measurements on the basis of a simplified electrical model of the adhesion contact.

Using this approach with rat hippocampal neurons in culture, the Kv2.1 conductance was demonstrated to be enhanced in the membrane adhering to the silicon oxide substrate (Antonucci et al. 2001). The extracellular voltage measured in these experiments was never large enough to affect channel gating significantly. The small amplitude of the voltage was derived from the relatively large distance, 50–100 nm, between the membrane and silicon oxide, from the low channel density in the cultured neurons, and from the low resistance of the adhesion cleft due to the small diameter of the cells.

We hypothesize that in a real neuron–astrocyte adhesion contact, instead, the extracellular voltage developing along the adhesion cleft affects the gating of Kv2.1 channels. In the mammalian brain the soma of the neurons is in contact with astrocytic processes. These are sites of cell–cell adhesion that can reach several micrometers in diameter and where the distance between the neuronal and glial membrane is only 20 nm. Voltage-dependent potassium channels Kv2.1 are highly accumulated in the neuronal membrane at these contact sites (Du et al. 1998). In addition, the specific electric resistance within the adhesion cleft, because of the extracellular matrix, might be higher than in a neuron–silicon junction.

In the present work we first validate experimentally an electrodiffusion-based model describing an adhesion cleft with voltage-gated channels. For this purpose we use *Xenopus* oocytes expressing recombinant *Shaker* potassium channels with removed inactivation (*ShIR*) (Yellen et al. 1991). After the oocyte is attached to the silicon oxide, the extracellular voltage along the cleft between the cell and substrate is measured, at different intracellular voltages, using a linear array of 96 transistors integrated in the silicon (Fig. 1). The measured voltages are compared with those computed on the basis of the model. Finally, we use the model, with appropriate parameters, to predict Kv2.1 gating along a neuron–astrocyte adhesion contact.

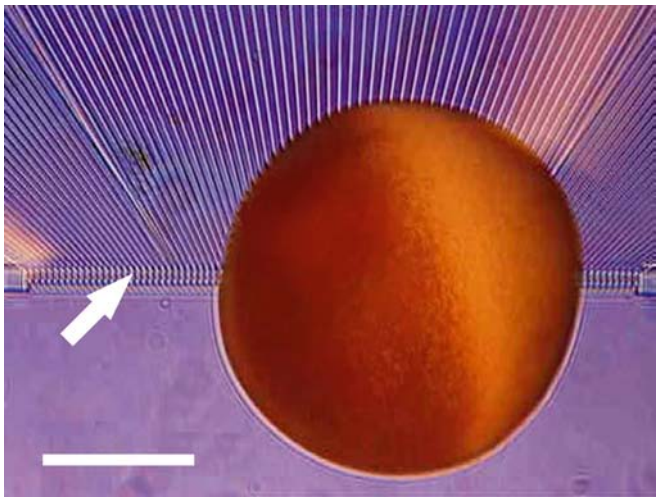

Fig. 1 Oocyte on transistors. Microphotograph of a *Xenopus* oocyte attached to a linear array of 96 transistors integrated in a silicon chip. Visible in the upper part of the figure are drain lanes. The *arrow* indicates one of the 96 gates (2×20 μm each) comprised of the drains and the common source. The oocyte covers a large part of them. The *scale bar* is 500 μm

Materials and methods

Oocytes

Oocytes were extracted from *Xenopus laevis* under general anesthesia through a small incision in the abdomen. Oocytes at maturation stage V–VI were isolated and the follicle cell layer removed after treatment with 1 mg/mL collagenase A (Sigma, Heidelberg, Germany) in OR I medium [(in mM): 82.5 NaCl, 2.5 KCl, 1.0 $MgCl_2$, 1.0 Na_2HPO_4, 5.0 HEPES (pH 7.5)]. They were then kept at 19 °C for 1–3 days in OR III medium [(in mM): 82.5 NaCl, 2.5 KCl, 1.0 $CaCl_2$, 1.0 $MgCl_2$, 1.0 Na_2HPO_4, 5.0 HEPES (pH 7.5)], with the addition of 50 mg/mL gentamycin (Boeringer, Germany) and 0.11 mg/mL sodium pyruvate (Sigma). Prior to electrophysiological recording with transistors, the vitelline envelope was mechanically removed following osmotic shrinkage of the oocyte in a solution containing (in mM): 200 potassium aspartate, 20 KCl, 1.0 $MgCl_2$, 5.0 EGTA, 5 HEPES (pH 7.5).

RNA synthesis and oocyte injection

The plasmid ShIR_pcDNA3 was obtained by subcloning the original *Shaker IR* (*ShIR*) mutant (Yellen et al. 1991) in the expression vector pcDNA3 (Invitrogen, Germany). RNA was synthesized after the plasmid was linearized with EcoRI and transcribed with T7 RNA polymerase (Promega, La Jolla, Calif., USA), as described by Methfessel et al. (1986). Each oocyte was then injected with about 50 nL of a 1 μg/μL RNA aqueous solution.

Silicon chip

Xenopus oocytes were attached onto chips with a linear array of 96 metal-free p-type field-effect transistors on n-type silicon with a lattice constant of 20 μm. The whole surface was covered with silicon dioxide. The length and width of a gate were 1.8 μm and 20 μm, respectively. The thickness of the silicon oxide in the gate region was 12 nm. The design of the linear array (Rentschler and Fromherz 1998) and its fabrication (Kiessling et al. 2000) were previously described.

Oocyte on silicon chip

A Perspex chamber (bottom diameter 3 mm) was attached to a silicon chip (1 cm×1 cm) with integrated transistors. The surface of the chip was wiped carefully with a 1% solution of a liquid dish detergent, rinsed with milli-Q water (Millipore, Bedford, Mass., USA) and dried. The chips were coated with poly-L-lysine (MW > 300,000; Sigma) by adsorption from a 20 μg/mL aqueous solution for 1 h and dried.

An oocyte without a vitelline envelope was positioned on the transistor array using a polished Pasteur pipette and left to adhere for 10 min before starting the electrophysiological recording. After this time the oocyte was strongly attached to the chip surface.

Electrophysiology: intracellular and extracellular recording

Two-electrode voltage clamp

Oocytes were impaled using intracellular pipettes with broken tips having a resistance below 1 MΩ and filled with 2 M KCl as described in Stuehmer (1998). The oocytes were voltage clamped using a TEC-10C amplifier (npi electronic, Tamm, Germany). Voltage protocols were applied and currents recorded through a PC running a custom-made program. The extracellular recording solution contained (in mM): 96 NaCl, 2 KCl, 1.8 $CaCl_2$, 1 $MgCl_2$, 5 HEPES (pH 7.3).

Recording with transistors

Recording with transistors was performed as previously described (Vassanelli and Fromherz 1999; Straub et al. 2001). Briefly, bias voltages were applied to the bulk silicon, to the common source and to the drains to define the working point of the transistors. Typically the working point of a transistor was in the range 0.8–1.0 V for the source-gate voltage and 0.6–0.8 V for the source-drain voltage. Bulk silicon was always kept at the source potential. The working point was chosen in order to have a linear relation between the source-drain current and the gate voltage over the whole experimental range. The slope of the relation was measured before and after each experimental session for each transistor. Only the measurements where the slope was constant were evaluated. Typically a change of 1 mV in the gate voltage induced a change of 0.1 μA in the source-drain current. We selected 36 transistors for measurements along the region beneath the oocyte. For a complete junction profile we often had to measure with 72 transistors in two successive runs.

AC voltage measurements

We derived the approach from one previously described (Weis and Fromherz 1997; Fromherz et al. 1999; Kiessling and Fromherz, unpublished work). The intracellular voltage was clamped to bias voltages ranging from −70 mV to 30 mV (5–10 mV interval). AC voltages $V_M(v)$ of frequency v (amplitude 5 mV) from 5 to 1000 Hz were superimposed on each bias voltage. The modulations of the 36 source-drain transistor currents were amplified and fed into 36 custom-made two-phase lock-in amplifiers, built-in SMD technique (Cicorel, Ismaning, Germany). In addition, the intracellular voltage and the whole-cell current were measured with two two-phase lock-in amplifiers (SR 830, Stanford Research Systems, Sunnyvale, Calif., USA) for determination of the whole-cell impedance. The bias voltages were clamped only long enough to allow reliable recording by the lock-in amplifiers. As a consequence, bias voltages were clamped, starting from a holding potential of −70 mV, for a minimum of 450 ms to a maximum of 3 s, depending on the frequency. Measurements were taken only after *ShIR* channel activation reached the steady state. It has to be noted that the lack of fast inactivation in these channels and their modest slow inactivation strongly reduced the interference of inactivation kinetics on these measurements. Even at the lowest frequencies, slow inactivation did not introduce a significant error. This was verified in non-adhering oocytes by comparing the voltage dependence of the steady-state potassium conductance and the time constant of activation obtained from whole-cell impedance measurements with those estimated from conventional pulses measurements and with the known gating curve of the channel (Yellen et al. 1991).

After normalizing the response of each transistor to a reference measurement without any cell, we obtained the complex frequency-dependent profiles of the AC extracellular voltage, $V_J(a,v)$, along the adhesion cleft (indicating with a the radial coordinate of the contact).

Whole-cell membrane parameters

As explained in the next section (Electrodiffusion model: channel gating in adhesion site), the voltage dependence of the *ShIR* potassium conductance and its activation kinetics were described by a simple electrical model that was derived for a related potassium conductance (Neher 1971). Although approximate with respect to

other available models (Zagotta and Aldrich 1990), it offered the advantage of simplifying the numerical simulations.

For each oocyte placed on a chip, the whole-cell membrane capacitance and leakage conductance were obtained both from pulses and impedance measurements while clamping the cell at an intracellular bias voltage of −70 mV.

Steady-state whole-cell potassium conductances at different intracellular voltages (Yellen et al. 1991), as well as time constants of activation, were obtained both from pulses and impedance measurements (Koch 1999) while clamping the cell at different intracellular bias voltages.

The whole-cell membrane area was computed from the oocyte diameter, assuming a spherical shape. The area of the membrane "free" from adhesion ("free" membrane) was defined as the difference between the whole-cell area and the area of the junctional membrane. The area of the junctional membrane was computed from the diameter of the junction, assuming a circular shape. The specific leakage conductance and capacitance were obtained by dividing the corresponding whole-cell values by the membrane area. It has to be noted that at the steady state the maximum specific potassium conductance was obtained by dividing the maximum whole-cell potassium conductance by the area of the "free" membrane alone, as explained in the next section.

The potassium reversal potential was derived from "tail currents" measured during repolarizing pulses after a test pulse to 20 mV. From the reversal potential we derived an estimate of the intracellular potassium concentration, C^{K}_{in}, assuming as extracellular potassium concentration, C^{K}_{out}, that of the extracellular recording medium.

We also measured the whole-cell membrane parameters and potassium reversal potentials in some oocytes with the vitelline envelope placed on a Sylgard-coated glass substrate. Under these conditions the oocyte membrane did not adhere to the substrate, allowing the determination of the steady-state activation curve and the voltage dependence of the time constant of activation in a membrane completely "free" from adhesion.

Theory

Electrodiffusion model: channel gating in adhesion site

The gating of ion channels in an adhered membrane depends on the voltage difference $V_M - V_J$, where V_M is the intracellular potential and V_J is the potential in the cleft between the cell membrane and the adhesion substrate (Fromherz 1999). If the adhesion substrate is an insulator, for example another cellular membrane or a layer of silicon oxide, the adhesion site can be electrically described as a two-dimensional cable with a distance d between the two insulating layers (Weis and Fromherz 1997).

Ionic fluxes through the adhering membrane are coupled to ionic fluxes along the cleft, as predicted by electrodiffusion theory (Straub 2001; Fromherz et al., unpublished work). Briefly, in the case of a circular adhesion contact, the two-dimensional cable is a cylinder of height d where the conductive electrolyte is comprised, as in a "sandwich", between the cell membrane and the silicon substrate. The ions permeating the adhering membrane through ionic channels generate ionic fluxes within the cleft which are regulated by drift and diffusion processes. We consider only drift and diffusion occurring in the two dimensions of the adhesion contact plane, while ions are assumed to distribute instantaneously along the distance d, which is typically only for some tens of nanometers. Let us consider an infinitely small volume, v, of electrolyte having height d and located arbitrarily along the cable. Ions moving into and out of v within a time interval δt will cause a net change of ionic concentrations, δC^{i}_{out}, with C^{i}_{out} representing the external concentrations of the ions of species i. According to electrodiffusion theory, ions are caused to flow into or out of v by (1) the concentration gradients and (2) the potential gradient. A third additional contribution is given by the ions permeating the adhering membrane through ion channels. Equation (1a) describes the change of ionic concentrations, $\delta C^{i}_{out}/\delta t$, within the elementary volume, v, as the sum of these three processes:

$$\frac{\partial C^{i}_{out}}{\partial t} = D^{i}\nabla^{2}C^{i}_{out} + \frac{z^{i}FD^{i}}{RT}\nabla\left(C^{i}_{out}\nabla V_J\right) + \frac{g^{i}_{JM}}{z^{i}Fd}\left(V_M - V^{i}_{0} - V_J\right) \quad (1a)$$

Accumulation or depletion of ions within v is associated with a corresponding change of electric charge which loads, or unloads, the capacities of the membrane and silicon oxide (Eq. 1b). It is important to note that Eq. (1b) is valid only when V_M is constant. Experimentally, this implies that the cell is voltage clamped at a constant intracellular voltage:

$$(c_M + c_S)\frac{dV_J}{dt} = Fd\sum_{i} z^{i}\frac{\partial C^{i}_{out}}{\partial t} \quad (1b)$$

Here D^{i} are the diffusion coefficients, g^{i}_{JM} are the specific ionic conductances of the adhering membrane, and V^{i}_{0} are the reversal potentials for ions of species i with valence z^{i}. c_M and c_S are the specific capacities of the membrane and silicon oxide, respectively (concentrations are expressed in mol/cm^3 if the space unit is cm).

The two coupled Eqs. (1a) and (1b) allow the computation of V_J, and of the associated extracellular ionic concentrations, for a given intracellular voltage in an arbitrary position of the adhesion site. The ionic conductances and the reversal potentials are here independent parameters. In the next section we introduce the effect of the extracellular voltage and ionic concentrations on g^{i}_{JM} and V^{i}_{0} and we develop a theoretical frame to predict the effect of adhesion on channel gating in our

experimental system: the oocyte silicon junction with *ShIR* potassium channels.

Channel gating in the oocyte–silicon adhesion site

In our experiments the two-dimensional cable was formed by the membrane of a *Xenopus* oocyte adhering to a thin insulating layer of silicon oxide. Transmembrane ionic currents were potassium currents, with g^{K}_{JM} depending on mutated *ShIR* potassium channels lacking inactivation expressed in the membrane of the oocyte.

We made four assumptions: (1) the oocyte–silicon junction has a cylindrical geometry, with the adhesion area having a circular shape of radius a_J; (2) the extracellular space between the membrane microvilli was contributing to the average distance, d, between the adhering membrane and the silicon oxide layer; (3) the channels in the adhering membrane have the same gating properties as in the "free" (i.e. non-adhering) membrane; (4) the channels have a homogeneous spatial distribution.

We restricted our model to steady-state conditions of transmembrane voltage. Since, in our experiments, V_M was kept constant, this implies that only conditions where g^{K}_{JM}, was computed using Eq. (2), according to a simple model describing the voltage dependence of a related conductance (Neher 1971):

$$g^{K}_{JM} = n^{3}_{J\infty} g_0 \tag{2}$$

Here g_0 is the maximum specific potassium conductance and $n^{3}_{J\infty}$ is the fraction of open channels in the junction at the steady state. $n^{3}_{J\infty}$ is related to the voltage across the membrane by Eq. (3) with the gating valence z_G, the Faraday constant F, the gating potential V_G and the Boltzmann term RT (Yellen et al. 1991):

$$n^{3}_{J\infty} = \frac{1}{1+\exp\left[\frac{z_G F(V_M - V_J - V_G)}{RT}\right]} \tag{3}$$

Again, the transmembrane voltage is given by the difference between the intracellular voltage, V_M, and the extracellular voltage along the junction, V_J.

The reversal potential for potassium ions, $V^{K}_{0}(a)$, is given by Eq. (4) with the intracellular concentration, C^{K}_{in}, and the local extracellular concentration, C^{K}_{out}:

$$V^{K}_{0} = \frac{RT}{F}\ln\left(\frac{C^{K}_{out}}{C^{K}_{in}}\right) \tag{4}$$

From Eqs. (1a, 2, 3, 4) it appears that V_J, g^{K}_{JM} and V^{K}_{0} are interdependent. Equations (1a, 2, 3, 4) were solved numerically by a simple Gaussian algorithm (Press et al. 1992). The starting external ionic concentrations in the cleft (we considered K^+, Na^+ and Cl^-) were those of the extracellular recording medium, while the intracellular potassium concentration was obtained as described in the electrophysiology methods section. The solution results in several position-dependent parameters in the cleft: the potential $V_J(a)$, the membrane conductance $g^{K}_{JM}(a)$, the external ion concentrations $C^{i}_{out}(a)$, the reversal potential $V^{K}_{0}(a)$ and the specific resistance of the electrolyte, $\rho(a)$ (Eq. 5), where a is the radial coordinate along the radius of the junction a_J:

$$\rho = \left[\sum_i \frac{F^2 z^{i^2}}{RT} D^i C^i_{out}\right]^{-1} \tag{5}$$

Additionally, we calculated the rate constants α_{Jn} and β_{Jn} in any point of the adhesion cleft with the empirical Eqs. (6) and (7) (voltages are expressed in mV):

$$\alpha_{Jn} = \frac{18(-(V_M - V_J) - 30)}{\exp\left(\frac{-(V_M - V_J) - 30}{10}\right) - 1} \tag{6}$$

$$\beta_{Jn} = 75\ \exp\left(\frac{-(V_M - V_J)}{30}\right) \tag{7}$$

The two relations were experimentally derived from the activation of the *ShIR* potassium conductance in the "free" membrane, where $V_J = 0$. They allowed us to compute the time constant of activation, $\tau_{Jn} = 1/(\alpha_{Jn} + \beta_{Jn})$, along the cleft.

As an example, we computed $g^{K}_{JM}(a, V_M)$ and $\tau_{Jn}(a, V_M)$ for a typical oocyte–silicon junction with *ShIR* channels (Fig. 2). There is a remarkable resulting "drop" of the steady-state potassium conductance in a very large area of the adhesion contact. The opening of potassium channels at depolarizing intracellular voltages generates an outward current which produces in the oocyte–silicon junction a double effect: (1) it creates a positive extracellular voltage, V_J, and (2) it increases the potassium concentration in the cleft, collapsing the reversal potential. With a feed-back mechanism, the positive extracellular voltage causes a drop of the transmembrane potential and a block of channel opening, while the collapse of the reversal potential reduces the potassium outward current and counteracts the development of the extracellular voltage. Once at steady state, the net effect of this interplay is that the dependence of the potassium conductance on the intracellular voltage is strikingly different in the free with respect to the adhering membrane: in the first one the steady-state potassium conductance increases with the intracellular voltage following the typical S-shaped gating curve; in the second one the potassium conductance is very low in a large portion of the adhesion contact, even for high intracellular voltages.

In the same contact area the time constant of activation remains high for depolarizing voltages, whereas it decreases in the free membrane, forming the typical bell-shaped curve. For simplicity's sake we did not include in this computation the leakage conductance of the oocyte membrane, which gives, anyway, a negligible contribution to the total membrane conductance.

It has to be noted that solving Eqs. (1a, 2, 3, 4) to determine the ionic concentration changes in the cleft implies a conceptually fundamental approximation: the

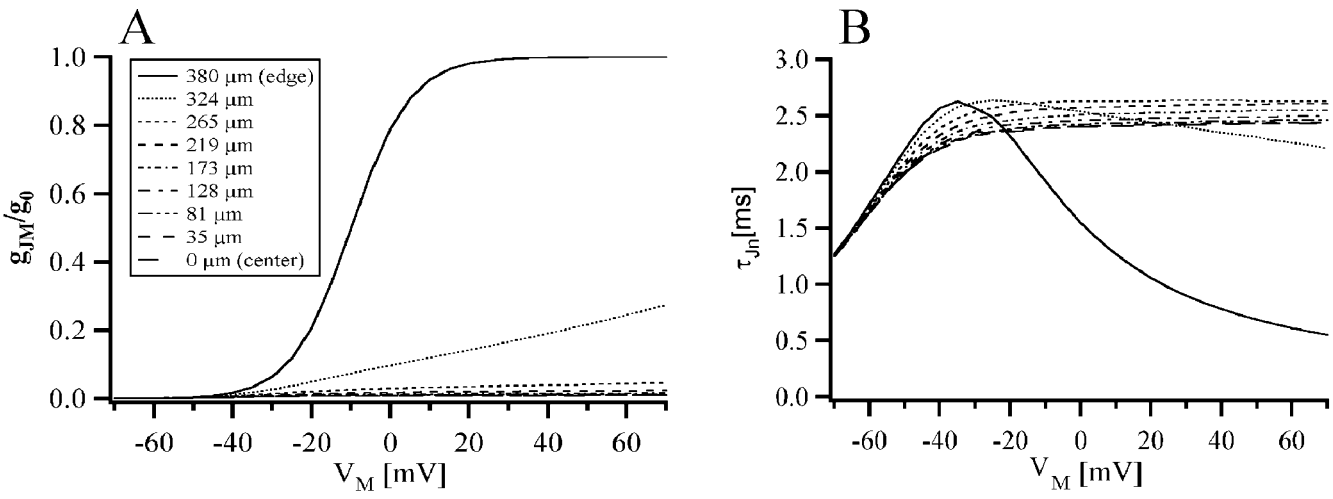

Fig. 2A, B g_{JM} and τ_{Jn} computed in a typical oocyte–silicon junction. **A** Gating curves of *ShIR* computed along the radius of a typical oocyte–silicon junction. The relative conductance at a given intracellular voltage was obtained by dividing the specific conductance (g_{JM}) by the maximum specific conductance (g_0) of 9.7 mS/cm^2. In Eq. (3) it was $z_g = 3.3$ and $V_G = -10$ mV. The radius of the junction, a_J, was 380 μm, and the width of the cleft was 152 nm. In the *inset* are indicated the distances from the center of the junction with the corresponding different line styles. **B** Time constants of activation of the *ShIR* conductance along the radius of the junction. The different curves are defined as in **A**

steady-state potassium conductance is assumed to reach instantaneously its value at any given transmembrane potential. Thus, the delay due to activation kinetics is assumed to play no role in the development of significant concentration changes in the adhesion cleft. We confirmed the validity of this assumption, at least for voltage pulses longer than 10 ms, by carrying out piloting numerical simulations, including the activation kinetics of the potassium conductance using the rate constants calculated with Eqs. (6) and (7).

We wanted to verify the theoretical model of potassium channel gating in adhesion, with its prediction of the steady-state potassium conductance and time constant of activation, by comparing numerical simulations with experimental recordings of V_J at the oocyte–silicon junction. Albeit generally used in conventional electrophysiology, we avoided the use of intracellular voltage pulses because they require numerical simulations of V_J kinetics, not implemented in our model, and a large computational load. Indeed, during voltage pulses and before reaching the steady state, V_J follows complex kinetics (Fig. 3) reflecting capacitive charging, potassium conductance activation, electrodiffusion dynamics and their interdependency. We adopted, instead, an experimental approach suitable to measure V_J when the electrodiffusion process was at the steady state and channel gating was independent from the dynamics of the extracellular potential and of the ionic concentration changes.

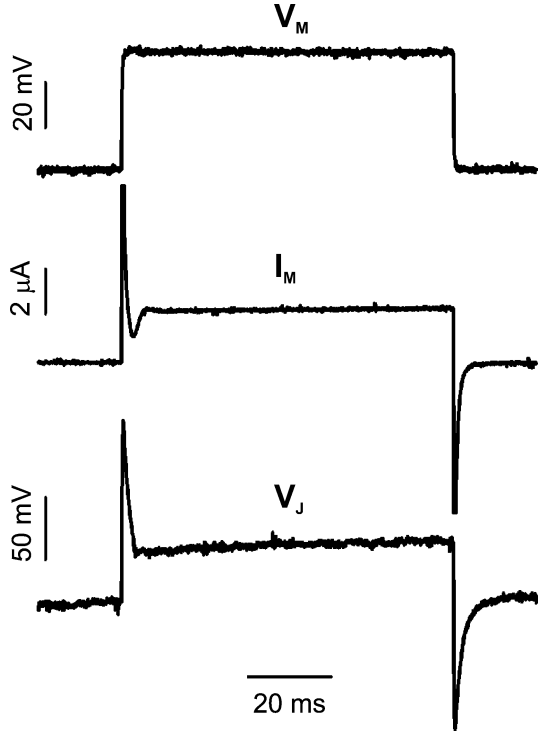

Fig. 3 V_J kinetics during intracellular voltage pulse. Representative recording of the extracellular voltage, V_J, in the center of a typical oocyte–silicon junction during a depolarizing intracellular voltage pulse to −20 mV. The intracellular voltage, V_M (*top*), the corresponding whole cell current, I_M (*middle*), and the extracellular voltage (*bottom*) are all shown. The intracellular pulse was started from a holding potential of −70 mV. The whole-cell current was corrected for leakage, but compensation and offline correction of capacitive currents were not performed, allowing a direct comparison of I_M and V_J. Notable is the difference between the kinetics of the whole-cell current and that of the extracellular voltage before reaching the steady state. The kinetics of the extracellular voltage results from a complex interplay between capacitive charging, potassium conductance activation and electrodiffusion dynamics within the adhesion cleft

AC voltage modulation: from electrodiffusion to the electric model

We estimated that small AC voltages superimposed on a constant bias intracellular voltage generate, per se,

negligible changes of extracellular potential and ionic concentrations within the oocyte–silicon junction. Thus, under AC modulation, channel gating can be assumed to be independent from electrodiffusion processes occurring within the cleft and the theoretical model describing channel gating in adhesion can be reduced to a simpler electric model. The approach is derived from Weis and Fromherz (1997) and Kiessling and Fromherz (unpublished work). We held the cell to constant intracellular bias voltages, V_M, and we modulated them by applying small AC voltages at different frequencies, $\underline{V}_M$. Bias voltages were held long enough to allow electrodiffusion of ions in the adhesion cleft to reach approximately the steady state. By measuring the extracellular voltages, $\underline{V}_J$, along the adhesion site, we obtained the experimental AC transfer, $h = \underline{V}_J/\underline{V}_M$.

The theoretical transfer function describing the AC transfer in the absence of voltage-dependent channels was derived previously (Weis and Fromherz 1997). The same function applies in our experiments to hyperpolarizing bias voltages where the contribution of voltage-dependent ion channels to the transfer is negligible: the junction is described by a "passive" cable and its sheet resistance, $r_J = \rho/d$, can be determined (Weis and Fromherz 1997).

At depolarizing bias voltages the contribution of voltage-dependent ion channels becomes important; using conventional terminology we say that the membrane undergoes a transition from a "passive" (i.e. voltage-independent) to an "active" (i.e. voltage-dependent) behavior. As a consequence, the electrical cable has to be modified with the introduction of the steady-state potassium conductance, g_{JM}^{K}, and two other "active" elements. Indeed, the potassium conductance response to small AC voltages can be described by linearized kinetic equations, thereby neglecting any additional changes of extracellular ion concentration (Hodgkin and Huxley 1952; Mauro et al. 1970; Koch 1999). The linearization of kinetic equations of first order results in the addition of a voltage-dependent inductance, l_{Jn}, and a second voltage-dependent conductance, g_{Jn}. The time constant of these elements is the time constant of potassium conductance activation, τ_{Jn}. These new parameters are related to the kinetic parameters α_{Jn} and β_{Jn} and the steady-state potassium conductance at the membrane potential V_M according to Eqs. (8) and (9):

$$\tau_{Jn} = \frac{l_{Jn}}{g_{Jn}} = \frac{1}{\alpha_{Jn} + \beta_{Jn}} \tag{8}$$

$$g_{Jn} = 3g_0 n_\infty^2 (V_M - V_J - V_0) \left.\frac{dn_\infty}{dV}\right|_{V_M - V_J} \tag{9}$$

For an intracellular voltage $\underline{V}_M$ of angular frequency $\omega = 2\pi\nu$ and with an additional membrane leakage conductance, g_{JM}^{leak}, we obtain the following differential equation for the complex voltage $\underline{V}_J$ in the cleft according to the two-dimensional electrical model in Fig. 4:

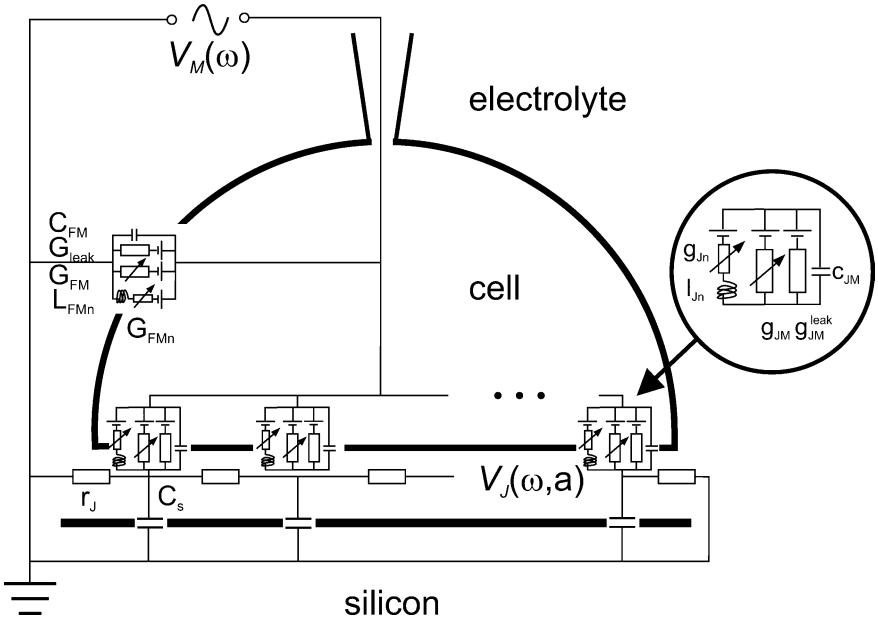

Fig. 4 Electrical model for small AC voltage modulations. The electrical scheme of an oocyte adhering to a silicon dioxide surface. In this cross-section, only one dimension of the cable is represented. The oocyte membrane and the silicon dioxide are depicted with *thick lines*. One of the two intracellular electrodes used to clamp the intracellular voltage, V_M, is sketched on top. The free membrane is described by a circuit element containing its total membrane capacitance, C_{FM}, leakage conductance, G_{leak}, *ShIR* conductances, G_{FM} and G_{FMn}, and inductance, L_{FMn}. Batteries indicate the reversal potentials of the ionic species flowing through the membrane. The adhering membrane is here represented by a series of similar circuit elements, each one describing an infinitely small patch of membrane. The local specific values of membrane capacitance, leakage conductance, *ShIR* conductances and inductance are indicated by c_{JM}, g_{JM}^{leak}, g_{JM}, g_{Jn} and l_{Jn}, respectively. The sheet conducting electrolyte between the membrane and silicon dioxide, having a total resistance r_J, is described by a series of resistances. The silicon dioxide, with a total capacity c_S, is represented by a series of capacitances

$$\frac{d}{\rho}\nabla \underline{V}_{\mathrm{J}} - \left[g_{\mathrm{JM}}^{\mathrm{K}} + g_{\mathrm{JM}}^{\mathrm{leak}} + i\omega(c_{\mathrm{JM}} + c_{\mathrm{S}}) + \frac{g_{\mathrm{Jn}}}{1 + i\omega\tau_{\mathrm{Jn}}}\right]\underline{V}_{\mathrm{J}} = -\left[g_{\mathrm{JM}}^{\mathrm{K}} + g_{\mathrm{JM}}^{\mathrm{leak}} + i\omega c_{\mathrm{JM}} + \frac{g_{\mathrm{Jn}}}{1 + i\omega\tau_{\mathrm{Jn}}}\right]\underline{V}_{\mathrm{M}} \tag{10}$$

The transfer function $h = \underline{V}_{\mathrm{J}}/\underline{V}_{\mathrm{M}}$ for a given position along the cleft can be easily calculated from this relation using a corresponding set of steady-state parameters obtained from the electrodiffusion model and from Eqs. (8) and (9). Thus, a good matching between the computed and experimental transfer functions at depolarizing intracellular voltages relies on the correct estimate of the steady-state potassium conductance and time constant of activation in adhesion by the electrodiffusion model. Equation (10) was computed numerically by successive overrelaxation (Press et al. 1992).

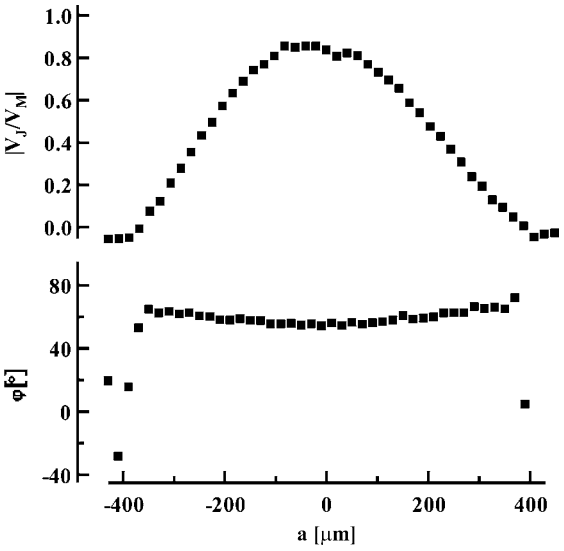

Fig. 5 Adhesion profile. Graphs showing the magnitude (*top*) and phase (*bottom*) profiles of an AC voltage transfer at 26 Hz for the same typical oocyte–silicon junction of Fig. 2. Each point is the recording of a single transistor. Evident in the phase are two rapid transitions, clearly indicating the two edges of the junction. The estimated radius of the junction was 380 μm

Results and discussion

Geometry of the junction and the "passive" parameters of the cable

The shape of the contact between the oocyte and silicon oxide was inferred from microscopic observations on standard glass coverslips coated with poly-L-lysine. The contact area of the oocyte on the glass was always approximately circular (not shown). This result was expected, considering the spherical shape of the oocyte, and it confirmed the validity of our previous assumption (1).

The radius of the junction, a_{J}, the resistance of the cleft, r_{J}, and the leakage membrane conductance, $g_{\mathrm{JM}}^{\mathrm{leak}}$, were determined from the transfer of small AC intracellular voltages along the cleft with a bias intracellular voltage of −70 mV. Under these conditions the contribution of the channels to the voltage transfer is negligible and the cable equation reduces to that of a "passive" cable (Weis and Fromherz 1997; Kiessling and Fromherz, unpublished work).

Radius

The AC transfer, particularly at high frequencies, is dominated by capacitive components. Starting from a few micrometers from the edge of the contact, the magnitude of the AC transfer rises rapidly, proceeding towards the center. The phase, on the other hand, rises suddenly at the edge of the junction at all frequencies. For these reasons the junction diameter becomes clearly visible in Fig. 5, where a typical experimental profile along the whole cleft at 26 Hz is shown in magnitude and phase. The radius of the oocyte adhesion contact to the silicon oxide was 380 μm. In contrast, the radius of the oocyte was 610 μm. In 23 different oocyte–silicon junctions the adhesion radius typically ranged from 300 to 500 μm, which was compatible with the size of oocytes at the V–VI stage of maturation. The radius of the junction was always smaller than the radius of the whole cell. The complete frequency profile, at −70 mV, is shown in Fig. 6A. Here a linear series of 36 transistors monitors the extracellular voltage in the cleft from the periphery to shortly after the center of the contact.

Resistance of the cleft and $g_{\mathrm{JM}}^{\mathrm{leak}}$

The resistance of the cleft, r_{J}, and the specific leakage membrane conductance, $g_{\mathrm{JM}}^{\mathrm{leak}}$, were obtained by fitting the magnitude and phase of the experimental AC transfer at −70 mV in the center of the junction. Indeed, with the radius of the adhesion area determined independently, the fitting in the center alone proved to be sufficient for a reliable estimate of these parameters. c_{S} was known to be 0.05 μF/cm^2 while for c_{JM} we chose a representative value giving a good fit to the experimental transfer at different intracellular bias voltages, from −70 mV to −10 mV. In the typical experiment shown in Fig. 6A we obtained $r_{\mathrm{J}} = 13$ MΩ and $g_{\mathrm{JM}}^{\mathrm{leak}} = 0.04$ mS/cm^2, with $c_{\mathrm{JM}} = 2.5$ μF/cm^2 compared to a whole-cell specific capcitance of 3.8 μF/cm^2.

The complete spatial profile of the AC transfer computed with the "passive" electrical cable model and these experimental parameters is shown in Fig. 7A. Experimental and fitting curves in the center are given in Fig. 8. The good agreement between the experimental (Fig. 6A) and theoretical (Fig. 7A) AC transfer profiles confirmed that the oocyte–silicon junction was well described by the electrical cable model.

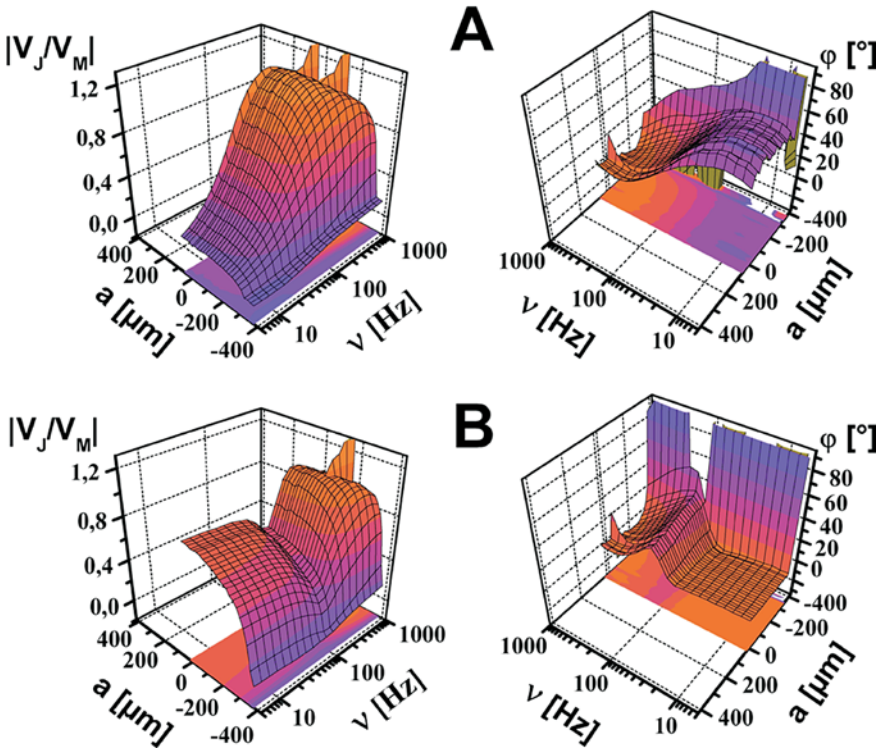

Fig. 6A, B Experimental AC transfer. Experimental radial profiles of the AC voltage transfer at different frequencies in a typical oocyte–silicon junction; the intracellular bias voltage was −70 mV in **A** and −20 mV in **B**. The magnitude, $|V_J/V_M|$, and phase, ϕ, of the AC transfer are plotted. The opening of the *ShIR* channels at −20 mV of intracellular voltage causes an increase of the magnitude and a decrease of the phase in the low-frequency range

Considering the different junctions we have investigated, we found the following ranges for the passive parameters: $r_J = 3$–$115\ \mathrm{M\Omega}$, $g_{JM}^{leak} = 0.01$–$0.05\ \mathrm{mS/cm^2}$ and $c_{JM} = 2$–$4\ \mu\mathrm{F/cm^2}$.

We repeated these measurements regularly during the experiments to check the state of cell adhesion and of membrane integrity. We always observed a progressive decrease of r_J, probably indicating a gradual loss of attachment of the oocyte with time.

The leakage conductance was usually identical in the adhering and in the whole-cell membrane. In a few cases we observed a large leakage conductance in the adhering

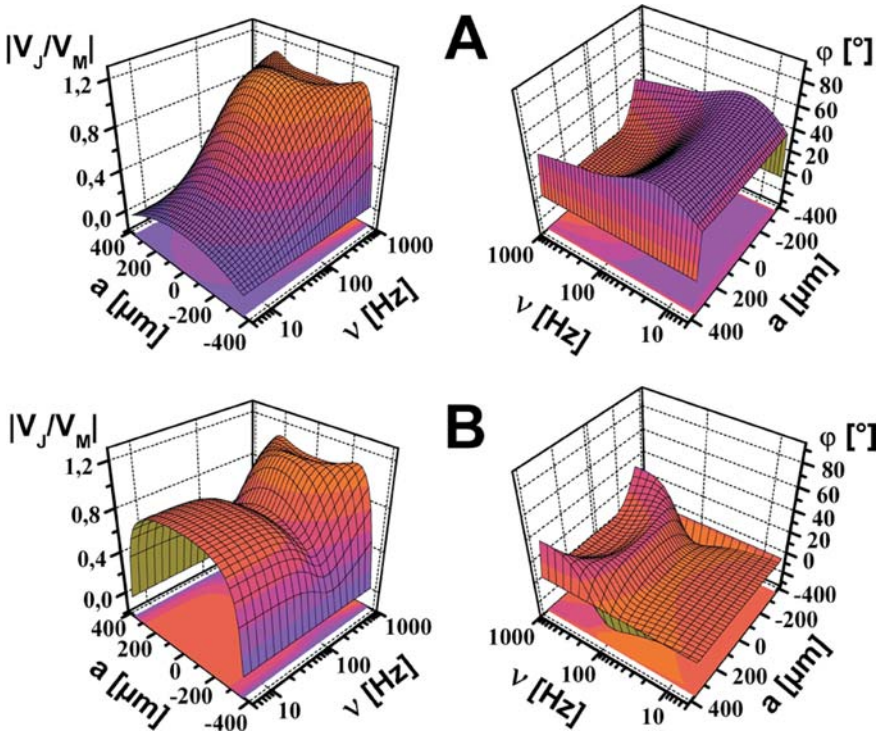

Fig. 7A, B Theoretical AC transfer. Computed spatial profiles of the AC voltage transfer at different frequencies in a typical oocyte–silicon junction. The parameters used for the computation are indicated in the text. As in Fig. 6, **A** and **B** are profiles computed at −70 mV and −20 mV of intracellular bias voltage, respectively. With respect to Fig. 6, the spatial profile is visible along the whole junction diameter

membrane, probably due to local membrane damage. c_{JM} was usually smaller than the whole-cell specific membrane capacitance; from this observation we might infer that the membrane microvilli were partially unfolded by adhesion.

From r_J we calculated the average distance between the membrane and silicon, assuming a specific resistance of the electrolyte in the cleft of 80 Ω cm, as in the bulk electrolyte. We obtained distances ranging from a minimum of 15 nm to a maximum of 600 nm, confirming the strong attachment of the oocyte to the silicon oxide surface. In the typical experiment shown in Fig. 6A the distance was 152 nm. These distances were comparable with those measured with a similar approach in the case of cultured cells on a silicon oxide surface coated with poly-lysine (Vassanelli and Fromherz 1997; Fromherz et al. 1999; Straub et al. 2001; Kiessling and Fromherz, unpublished work) and confirmed using optical methods (Braun and Fromherz 1998; Sonnleitner et al. 2002).

The "active" parameters of the junction

We measured the transfer of the small AC intracellular voltages along the cleft at depolarizing bias voltages ranging from −60 mV to 30 mV, with an increment of 5–10 mV. The experimental AC transfer at a representative depolarizing bias voltage of −20 mV is shown in Fig. 6B.

The transition that the AC transfer undergoes when the membrane is depolarized is evident both in the magnitude and in the phase. The opening of the channels at depolarizing bias voltages causes an increase of the extracellular voltage in the cleft in the low-frequency range where the magnitude now approaches unity. The maximum of the phase shift is decreasing and the onset is shifting to higher frequencies.

The experimental transfer changes along the diameter of the junction according to its cable properties. The maximum transfer occurs in the center of the adhesion site and drops to zero at the periphery. It is noteworthy that at a depolarizing bias voltage the magnitude of the AC transfer approaches unity for a very large area around the center of the junction over the whole frequency range.

Steady-state potassium conductance and time constant of activation in the oocyte–silicon junction

We investigated if the experimental transfer at depolarizing intracellular voltages was in agreement with our theoretical model of channel gating in adhesion based on cable and electrodiffusion theory (Fig. 2). We computed the AC transfer using the electrodiffusion and electric cable model with ionic channels (Eqs. 1a, 2, 3, 4, 5, 6, 7, 8, 9, 10). The maximum steady-state specific potassium conductance, g_0, was estimated by dividing the whole-cell steady-state maximum potassium conductance by the area of the sole "free" membrane. Indeed, as shown previously (Fig. 2) for the same typical oocyte–silicon junction, the computed steady-state potassium conductance is expected to be very low in most parts of the adhering membrane, even for large depolarizations. We obtained $g_0 = 9.7$ mS/cm^2. Typically its value ranged from 4 to 15 mS/cm^2, reflecting different channel densities in the different oocytes measured.

The computed transfer function is shown in Fig. 7B for the same representative depolarizing bias voltage as in Fig. 6B. The experimental and computed AC transfer profiles are similar both in magnitude and in phase.

The experimental and computed AC transfers in the center of the junction at different depolarizing bias voltages are shown in Fig. 8. For comparison we have also plotted in Fig. 8 the curves computed assuming that the potassium conductance in the junction was not affected by the potassium concentration changes and the

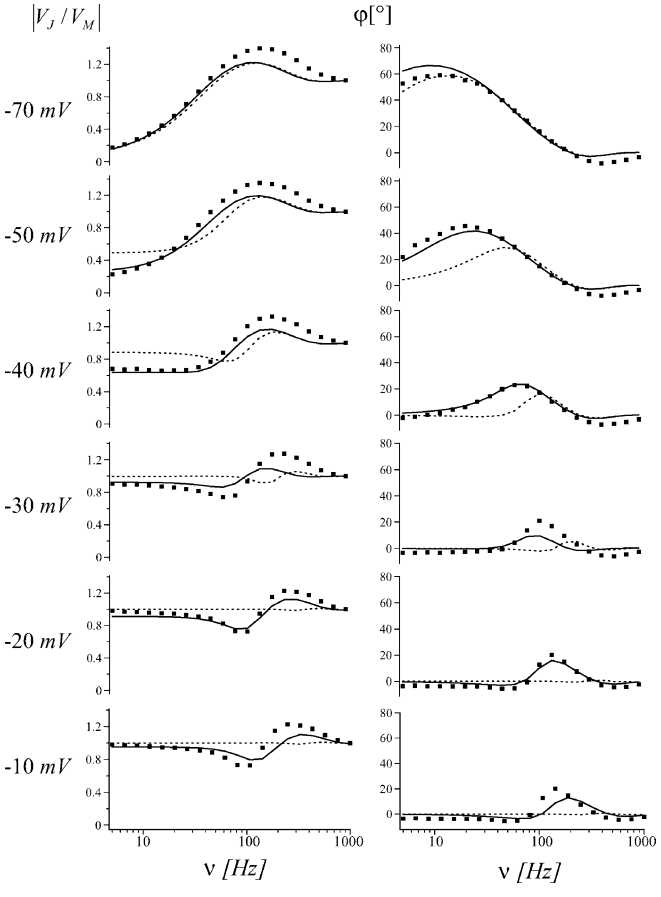

Fig. 8 Experimental and theoretical AC transfer in the center of the junction. The magnitude and phase of the AC voltage transfer in the center of the typical oocyte–silicon junction are plotted versus the frequency at different intracellular bias voltages. *Squares* are the experimental data; the *continuous line* is the AC transfer computed with Eqs. (1a, 2, 3, 4, 5, 6, 7, 8, 9, 10). The *dashed line* is the AC transfer computed assuming that the extracellular voltage in the junction, V_J, had no effect on channel gating (i.e. assuming V_J equals zero and $C^K_{out} = 2\times10^{-6}$ mol/cm^3)

extracellular voltage developing in the cleft (i.e. assuming $C^{K}_{out} = 2\times10^{-6}$ mol/cm^3 and $V_J = 0$ V as in the "free" membrane). The experimental and theoretical transfers are in good agreement only if the extracellular concentration and voltage changes are taken into account. This definitely demonstrates that channel gating at the oocyte–silicon junction differs in adhesion with respect to the free membrane: a positive extracellular voltage, V_J, develops within the oocyte–silicon cleft because of electrodiffusion processes; this affects the transmembrane potential and, consequently, channel gating, as predicted in Fig. 2.

We found a good agreement between the model and experiment in all our measurements, where junctions with different size and density of channels were investigated. Even for the lowest channels density, corresponding to 4 mS/cm^2 of membrane conductance, and for the largest membrane–silicon distance, around 600 nm, the effect of adhesion on channel gating was still significant (not shown). This result shows that the wide contact area of the oocyte on the silicon gives an important contribution to the development of a large extracellular voltage and to the consequent effect of adhesion on channel gating.

At the first sight it might be surprising that, despite the dramatic decrease of potassium conductance in a large and central region of the adhering membrane, the magnitude of the transfer function approaches unity in the whole junction. The result is understandable when considering that the junction has the properties of a core-conductor cable, where the maximum voltage transfer occurs in the center.

It is noteworthy that the potassium concentration changes in the cleft during the application of depolarizing bias intracellular voltages can be relatively large. For example, a depolarization to −20 mV for 1 s produces an increase of potassium concentration from 2×10^{-6} mol/cm^3 to 6×10^{-6} mol/cm^3 in the center of the junction.

From these results we could conclude that the electrodiffusion cable model with voltage-dependent channels was suitable to describe potassium channel gating along an adhesion cleft.

The imperfect correspondence of the theoretical curves with the experimental data might be caused by several reasons. We consider the following of note. First, we assumed that the junction had the shape of a cylinder with radius a_J and height d. We confirmed the circular shape of the adhesion but the average distance, d, between the membrane and substrate might have been inhomogeneous along the junction. Second, if the extracellular space between neighboring microvilli was sufficiently narrow, a local potassium accumulation and extracellular potential might have developed, particularly in the bottom of the folds, thus further affecting channel gating. With microvilli of about 1–2 μm length, we estimated that only a distance of a few tens of nanometers between neighboring microvilli might lead to significant changes in extracellular potassium concentration and extracellular voltage. Judging from scanning electron microscopy images, the distance between the microvilli appears to be larger (Sonnleitner et al. 2002). In addition, the attachment to the silicon substrate might have partially unfolded the membrane, similarly to what has been suggested to occur in cell-attached macropatches (Grigoriev et al. 1999), thus increasing the extracellular space between the microvilli and reducing the risk of potassium accumulation. Third, we assumed that the channels were homogeneously distributed. Probably they were not (Stuehmer 1998), but rather accumulated in clusters. However, the length constant of the cable (40 μm with open channels and >1000 μm with closed channels) was larger than the distance between the clusters and our assumption was held to a good approximation. Fourth, the slow inactivation of channels during the application of depolarizing bias voltages might have affected the steady-state potassium conductance and, therefore, the experimental measurements of the transfer functions. We demonstrated that this error was negligible by comparing whole-cell impedance and pulse measurements as described in the "Whole-cell membrane parameters" subsection of the electrophysiological methods section. In addition, as shown in Fig. 8, the magnitude of the experimental transfer function at bias voltages above −40 mV is almost constant for all frequencies below 20 Hz. If slow inactivation plays a significant role, the magnitude of the transfer function should decrease with the frequency in these measurements. The result is confirmed by the very modest slow inactivation reported for the *ShIR* channel in a previous study for the range of depolarizing voltages employed in our experiments (Yang et al. 1997). The same study excludes a possible significant modulation of the *ShIR* inactivation kinetics by extracellular potassium.

According to these considerations, the weak deviations observable in Fig. 8 could be possibly addressed in the theoretical model: a first improvement would be to condense the potassium conductance in membrane patches regularly distributed in the junction membrane. This would better reproduce the clustered distribution of potassium channels in oocytes, providing a more accurate description of current inflow and propagation within the cable, especially at depolarizing potentials. In addition, folds due to microvilli might be considered in the geometry of the cable and the slow inactivation kinetics included in the computation of the potassium membrane conductance. Unfortunately, these corrections would lead, as a side effect, to a significant increase of computation complexity.

It has to be clearly stated that the modulation of channel gating by adhesion that we have observed is only "apparent". The intrinsic voltage dependence of channel gating remains unchanged (assumption 3); gating is affected only by the local extracellular potential which modifies the transmembrane voltage. Thus, our theoretical model is generally applicable to all voltage-dependent ion channels in adhesion: the model does not rely on the specific gating properties of a particular

channel, provided that Eqs. (2), (3) and (6), (7) are substituted with those describing the voltage dependence of the steady-state conductance and time constant of activation of the ionic channel under consideration. For example, the effect of adhesion on the gating properties of a mutated non-inactivating sodium channel were observed experimentally at the oocyte–silicon contact and correctly described by the model (Vassanelli et al., unpublished work).

The effect on channel gating of the extracellular voltage developing between two adhering cells might be important in the physiology of the nervous system. In the following section, on the basis of experimental data and computations, we evaluate if this might be the case for potassium channel gating within a neuron–glia contact.

Kv 2.1 gating in a neuron–glia adhesion contact

We applied the electrodiffusion cable model to describe the gating of the potassium Kv2.1 conductance in a typical neuron–astrocyte adhesion contact of the mammalian central nervous system. In these contact regions, Kv2.1 channels accumulate to form high-density patches (Du et al. 1998). A similar accumulation of these channels occurs also in cultured neurons at the neuron–substrate interface, with an enhancement of the corresponding delayed rectifier potassium conductance in adhesion by a factor of 10 (Vassanelli and Fromherz 1999; Antonucci et al. 2001). With a similar factor of enhancement in the tissue, we have estimated the specific maximum potassium conductance at the neuron–astrocyte interface at around 50 mS/cm^2.

The radius taken for the contact was $a_J = 5$ μm. A typical contact between a single astrocytic process and the neuronal soma is smaller, as well as the area of channel accumulation (0.3–2 μm diameter) (Du et al. 1998). However, adjacent astrocytic processes are typically sealed by gap junctions and are likely to form adhesion contacts of larger diameter (Rash et al. 1997; Du et al. 1998). The distance, d, between the two adherent membranes is typically 20 mm. A major uncertainty concerns the value of the specific resistance of the extracellular fluid, ρ, within the cleft. According to different estimates, its value should range from 100 to 500 Ω cm, as assumed for a related model of a synaptic cleft (Savtchencko et al. 2000). We made, therefore, different computations covering the whole range. The specific capacities of the neuronal and astrocytic membranes were assumed identical, with a value of 1 μF/cm^2. The potassium reversal potential was assumed to be –75 mV. The steady-state Kv2.1 specific potassium conductance for a given transmembrane voltage was computed using Eqs. (2) and (3) with appropriate parameters (Murakoshi and Trimmer 1999) and pulse lengths of 10 ms. As mentioned before, we neglected the activation kinetics of the channels. This was confirmed with numerical calculations that included the kinetics.

It has to be recalled that the two-dimensional cable model we used implies an homogeneous distribution of the channels. This is apparently in contrast to the distribution in clusters of Kv2.1 in adhesion (Antonucci et al. 2001). However, the length constant of the cable is larger than the distance between the clusters and the effect of the inhomogeneous distribution of the channels becomes negligible.

The voltage dependence of the specific steady-state Kv2.1 potassium conductance along the adhesion contact is shown in Fig. 9A for a specific resistance of about 480 Ω cm in the cleft. There is evident a drop of the

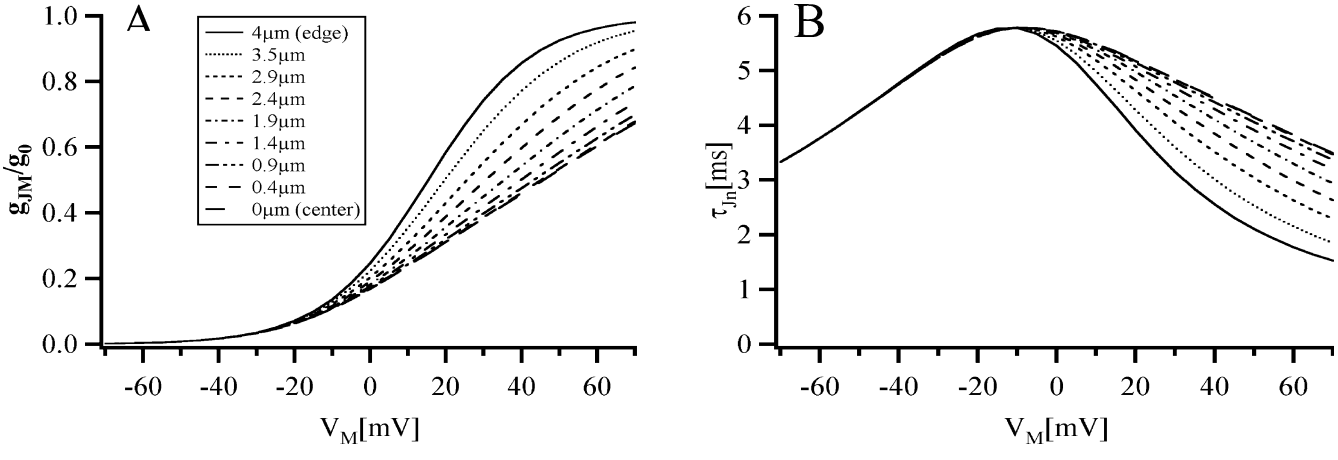

Fig. 9A, B Kv2.1 gating in a neuron-astrocyte contact. **A** Computed gating curves of Kv2.1 along the radius of a neuron–astrocyte adhesion contact. The maximum specific conductance, g_0, was 50 mS/cm^2, and the intracellular and extracellular potassium concentrations were 5×10^{-6} mol/cm^3 and 140×10^{-6} mol/cm^3, respectively. The extracellular sodium and chloride concentrations were 135×10^{-6} mol/cm^3 and 120×10^{-6} mol/cm^3, respectively. The diffusion coefficients of the external ions were proportionally reduced with respect to a physiological solution in order to obtain a specific resistance within the cleft of about 480 Ω cm. The bias intracellular depolarizations were 10 ms long. The radius of the contact was 5 μm. In Eq. (3) it was $z_g = 2.2$ and $V_G = -15.3$ mV. In the *inset* are indicated the different distances from the center of the contact and the line styles of the corresponding curves. **B** Time constants of activation of the Kv2.1 conductance along the radius of the adhesion contact. The different curves are defined as in **A**

membrane Kv2.1 conductance due to the adhesion, especially in the central part of the cleft.

We calculated also the voltage dependence of the time constant of activation: it is shown in Fig. 9B for the same specific resistance within the cleft. In order to describe the voltage dependence of the time constant of activation of Kv2.1, we adopted the model developed by Hodgkin and Huxley (1952) for the delayed-rectifier potassium conductance. Indeed, using KC blocking antibodies to identify the Kv2.1 conductance in cultured hippocampal neurons (Murakoshi and Trimmer 1999; Antonucci et al. 2001), we found that this model described the experimental kinetics with sufficient approximation. The computation shows that for depolarizing intracellular voltages the time constant is significantly larger in the neuron–astrocytic cleft than in the rest of the membrane. The effect is particularly evident in the central part of the contact.

We made the computation also with a specific resistance within the cleft of 70 Ω cm: the effect of the extracellular voltage on the gating of Kv2.1 was still significant. With a specific resistance greater than 480 Ω cm, the effect on channels gating was dramatic (not shown).

These findings may have important implications for the physiology of neurons in the brain. Kv2.1 potassium channels are involved in neuronal excitability, particularly during the repolarization phase of the action potential. Thus, according to our results, adhesion between neurons and astrocytes may affect neuronal excitation. By reducing the Kv2.1 conductance during depolarization, adhesion between the neuronal membrane and the surrounding astrocytes may significantly reduce the inward potassium current in the repolarization phase of the action potential. This might produce an increase of the amplitude of the action potential and slow down its repolarization phase. It is tempting to postulate that adhesion between glia cells and neurons and its effect on the gating of voltage-dependent channels represent a more general mechanism to regulate neuronal activity within the mature nervous system and during its development.

Acknowledgements We thank Prof. P. Fromherz for his support and critical reading of the manuscript, and Dr U. Fisher, Dr J. Kupper and Dr C. Oppawsky for introducing us to the techniques for manipulation, channel expression and electrophysiological recording of *Xenopus* oocytes.

References

Antonucci DE, Lim ST, Vassanelli S, Trimmer JS (2001) Dynamic localization and clustering of dendritic Kv2.1 voltage-dependent potassium channels in developing hippocampal neurons. Neuroscience 108:69–81

Braun D, Fromherz P (1998) Fluorescence interferometry of neuronal cell adhesion on microstructured silicon. Phys Rev Lett 81:5241–5244

Clay JR (1998) Excitability of the squid giant axon revisited. J Neurophysiol 80:903–913

Du J, Tao-Cheng JH, Zerfas P, McBain C (1998) The K + channel, Kv2.1, is apposed to astrocytic processes and is associated with inhibitory postsynaptic membranes in hippocampal and cortical principal neurons and inhibitory interneurons. Neuroscience 84:37–48

Frankenhaeuser B, Hodgkin AL (1956) The aftereffects of impulses in the giant nerve fibers of *Loligo*. J Physiol (London) 131:341–376

Fromherz P (1997) Self-gating of ion channels in cell adhesion. Phys Rev Lett 78:4131–4134

Fromherz P (1999) Extracellular recording with transistors and the distribution of ionic conductances in a cell membrane. Eur Biophys J 28:254–258

Fromherz P, Kiessling V, Kottig K, Zeck G (1999) Membrane transistor with giant lipid vesicle touching a silicon chip. Appl Phys A 69:571–576

Grigoriev NG, Spafford JD, Spencer AN (1999) The effects of level of expression of a jellyfish *Shaker* potassium channel: a positive potassium feedback mechanism. J Physiol (London) 517:25–33

Hodgkin A, Huxley AF (1952) A quantitative description of membrane current and its application to conduction and excitation in nerve. J Physiol (London) 117:500–544

Inoue I, Tsutsui I, Brown ER (1997) K + accumulation and K + conductance inactivation during action potential trains in giant axons of the squid *Sepioteuthis*. J Physiol (London) 500:355–366

Kiessling V, Müller B, Fromherz P (2000) Extracellular resistance in cell adhesion measured with a transistor probe. Langmuir 16:3517–3521

Koch C (1999) Biophysics of computation. Information processing in single neurons. Oxford University Press, New York

Mauro A, Conti F, Dodge F, Schor R (1970) Subthreshold behavior and phenomenological impedance of the squid giant axon. J Gen Physiol 55:497–523

Methfessel C, Witzemann V, Takahashi T, Mishina M, Numa S, Sakmann B (1986) Patch clamp measurements on *Xenopus laevis* oocytes: currents through endogenous channels and implanted acetylcholine receptor and sodium channels. Pflugers Arch 407:577–588

Murakoshi H, Trimmer JS (1999) Identification of the Kv2.1 K^+ channel as a major componenet of the delayed rectifier K^+ current in rat hippocampal neurons. J Neurosci 19:1728–1735

Neher E (1971) Two fast transient current components during voltage clamp on snail neurons. J Gen Physiol 58:37–53

Press WH, Flannery BP, Teukolsky SA, Vetterling WT (1992) Numerical recipies in C. Cambridge University Press, Cambridge, UK

Rash JE, Duffy HS, Dudek FE, Bilhartz BL, Whalen LR, Yasumura T (1997) Grid-mapped freeze-fracture analysis of gap junctions in gray and white matter of adult rat central nervous system, with evidence for a ''panglial syncytium'' that is not coupled to neurons. J Comp Neurol 388:265–292

Rentschler M, Fromherz P (1998) Membrane-transistor cable. Langmuir 14:547–551

Savtchenko LP, Antropov SN, Korogod SM (2000). Effect of voltage drop within the synaptic cleft on the current and voltage generated at a single synapse. Biophys J 78:1119–1125

Smith DO (1983) Extracellular potassium levels and axon excitability during repetitive action potentials in crayfish. J Physiol (London) 336:143–157

Sonnleitner A, Mannuzzu LM, Terakawa S, Isacoff EY (2002) Structural rearrangements in single ion channels detected optically in living cells. Proc Natl Acad Sci USA 99:12759–12764

Straub B (2001) Kopplung von Feldeffekttransistoren mit rekombinanten Ionenkanälen. PhD Dissertation, TU Munich, Germany

Straub B, Meyer E, Fromherz P (2001) Recombinant maxi-K channels on transistor, a prototype of iono-electronic interfacing. Nat Biotechnol 19:121–124

Stuehmer W (1998) Electrophysiologic recordings from *Xenopus* oocytes. Methods Enzymol 293:280–300

Vassanelli S, Fromherz P (1997). Neurons from rat brain coupled to transistors. Appl Phys A 65:85–88

Vassanelli S, Fromherz P (1999) Transistor probes local potassium conductances in the adhesion region of cultured rat hippocampal neurons. J Neurosci 19:6767–6773

Weis R, Fromherz P (1997) Frequency dependent signal transfer in neuron transistors. Phys Rev E 55:877–889

Yang Y, Yangyang Y, Sigworth FJ (1997) How does the W434F mutation block current in shaker potassium channels? J Gen Physiol 109:779–789

Yellen G, Jurman ME, Abramson T, MacKinnon R (1991) Mutations affecting internal TEA blockade identify the probable pore-forming region of a K+ channel. Science 4996:939–942

Zagotta WN, Aldrich RW (1990) Voltage-dependent gating of *Shaker* A-type potassium channels in *Drosophila* muscle. J Gen Physiol 95:29–60

Zhou L, Chiu SY (2001) Computer model for action potential propagation through branch point in myelinated nerves. J Neurophysiol 85:197–210